Supplement of Atmos. Meas. Tech., 10, 3429–3452, 2017
https://doi.org/10.5194/amt-10-3429-2017-supplement

Atmospheric Measurement Techniques
Open Access
EGU

Supplement of

Methane emissions from a Californian landfill, determined from airborne remote sensing and in situ measurements

Sven Krautwurst et al.

Correspondence to: Sven Krautwurst (krautwurst@iup.physik.uni-bremen.de)

S1 MAMAP remote sensing measurments (Google Earth overlays and single tracks)

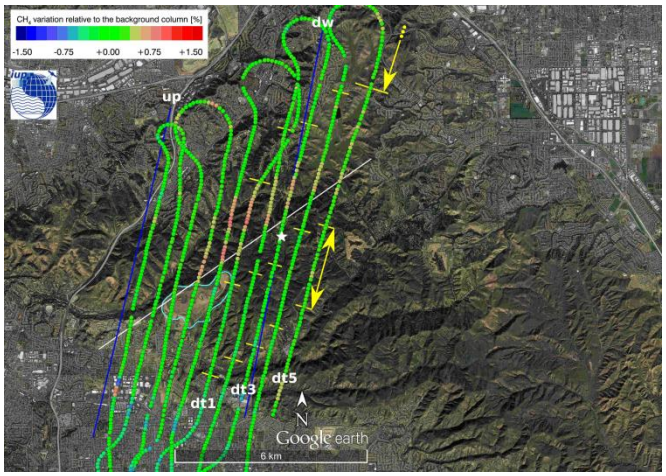

Figure S 1. As Fig. 6 (a) in the main part but for the 27.08.2014 and the star corresponds to the origin used for the in-situ walls in Figs. S5 (c,d) and S9 (a).

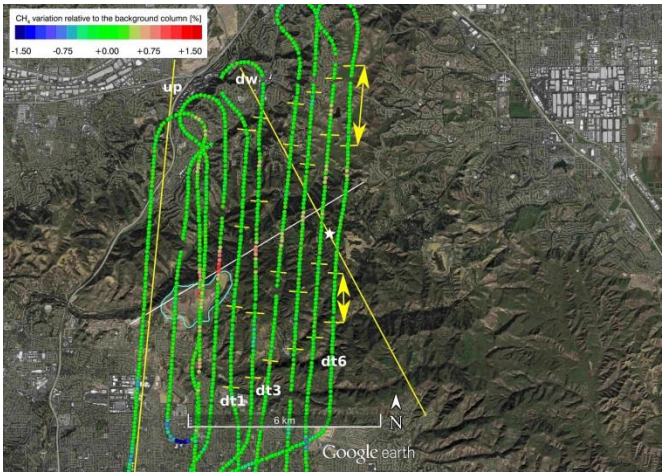

Figure S 2. As Fig. 6 (a) but for the 28.08.2014 and the star correspond to the origin used in Figs. S6 (c,d) and S9 (b).

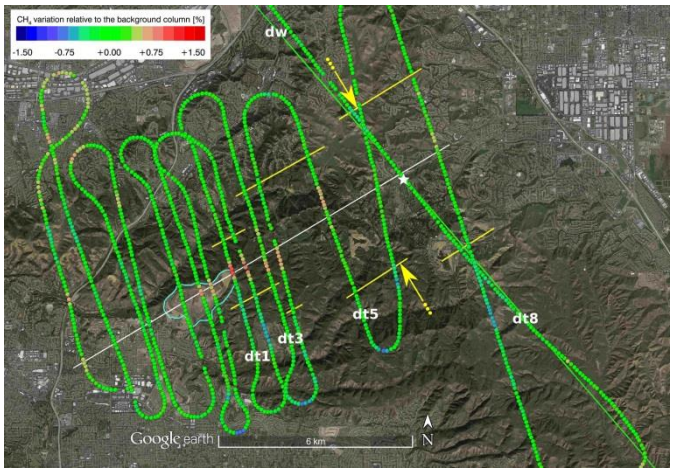

Figure S 3. As Fig. 6 (a) but for the 03.09.2014 and the star correspond to the origin used in Figs. S8, S9 (c).

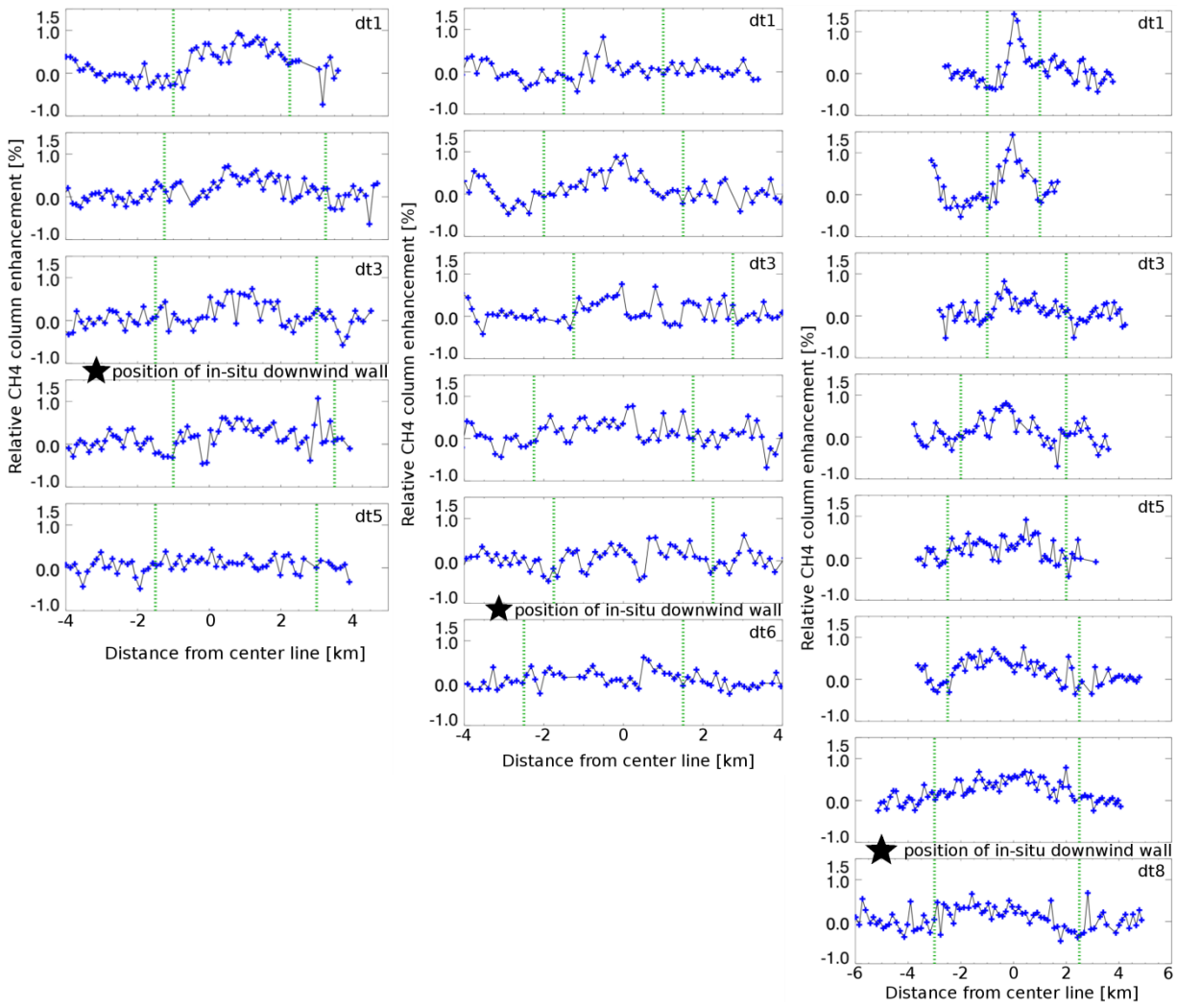

Figure S 4. As Fig. 7 (left column) but for the three other days (from left to right): 27.08.2014, 28.08.2014 and 03.09.2014.

S2 Picarro in-situ dry gas mixing ratios of CH_4

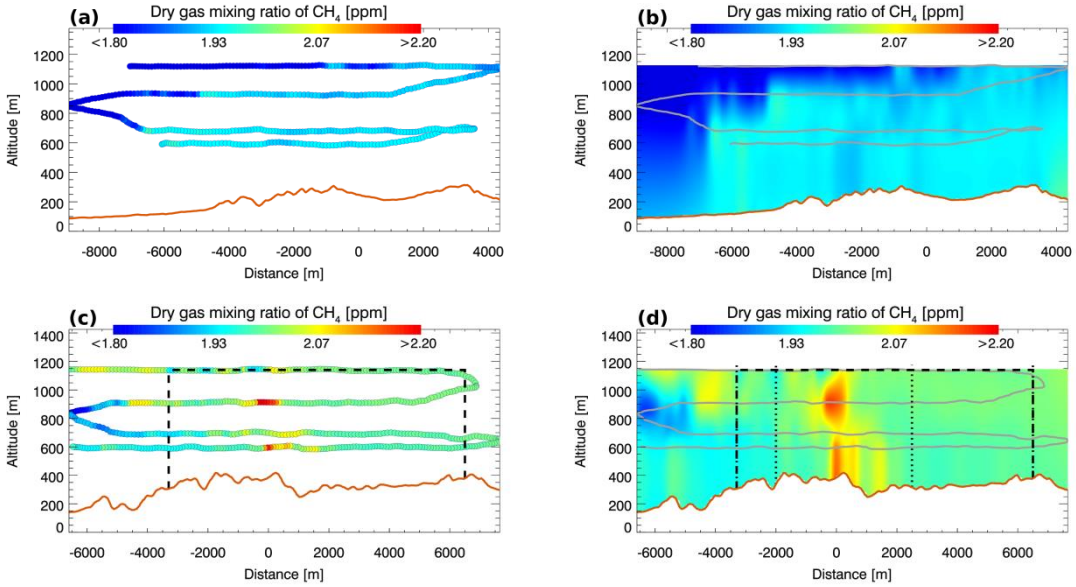

Figure S 5. Dry gas mixing ratios of CH_4 for the upwind (a,b) and downwind (c,d) wall on 27.08.2014. X-axis gives the distance from the approximate plume centre in m (only for bottom panels) and y-axis gives the altitude in m above sea level (m asl). Solid orange line depicts the surface elevation at the position of the wall (based on SRTM). Dashed black line depicts the area, which was used in the mass balance approach for estimating the emission rate. Dotted black line shows limits, which were used to define the background area (here: from - 3300 to - 2000 m and 2500 to 6500 m). Solid grey line depicts the flight track. (a,c) Measured dry gas mixing ratios of CH_4 along the flight track. Each circle represents one measurement. (b,d) Kriged dry gas mixing ratios of CH_4 based on the measurements shown in (a) and (b) and an additionally added pseudo surface track (not shown).

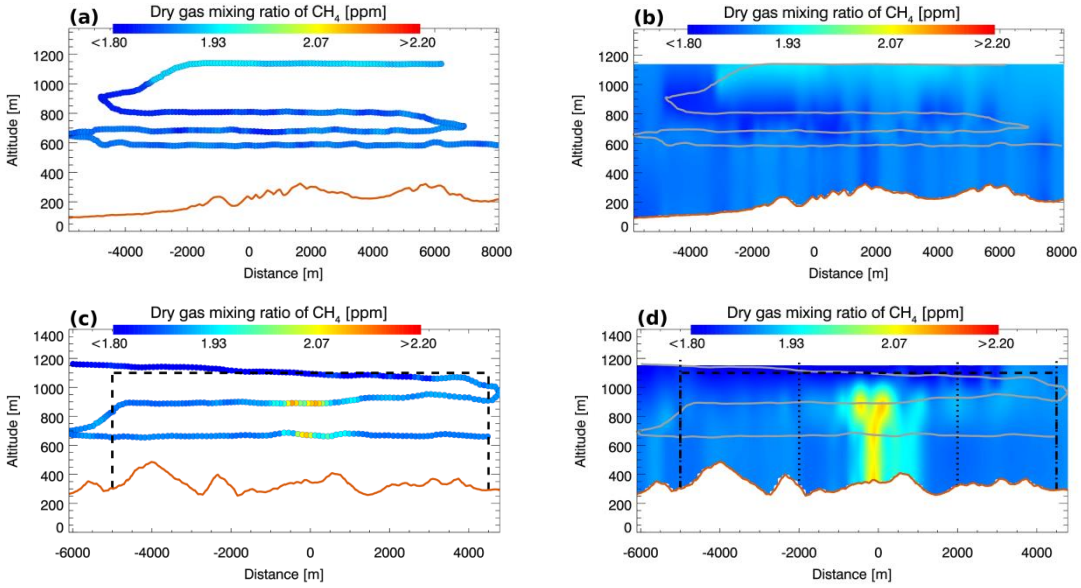

Figure S 6. As for Fig. S5 but for the 28.08.2014. (a,b) Upwind wall. (c,d) Downwind wall.

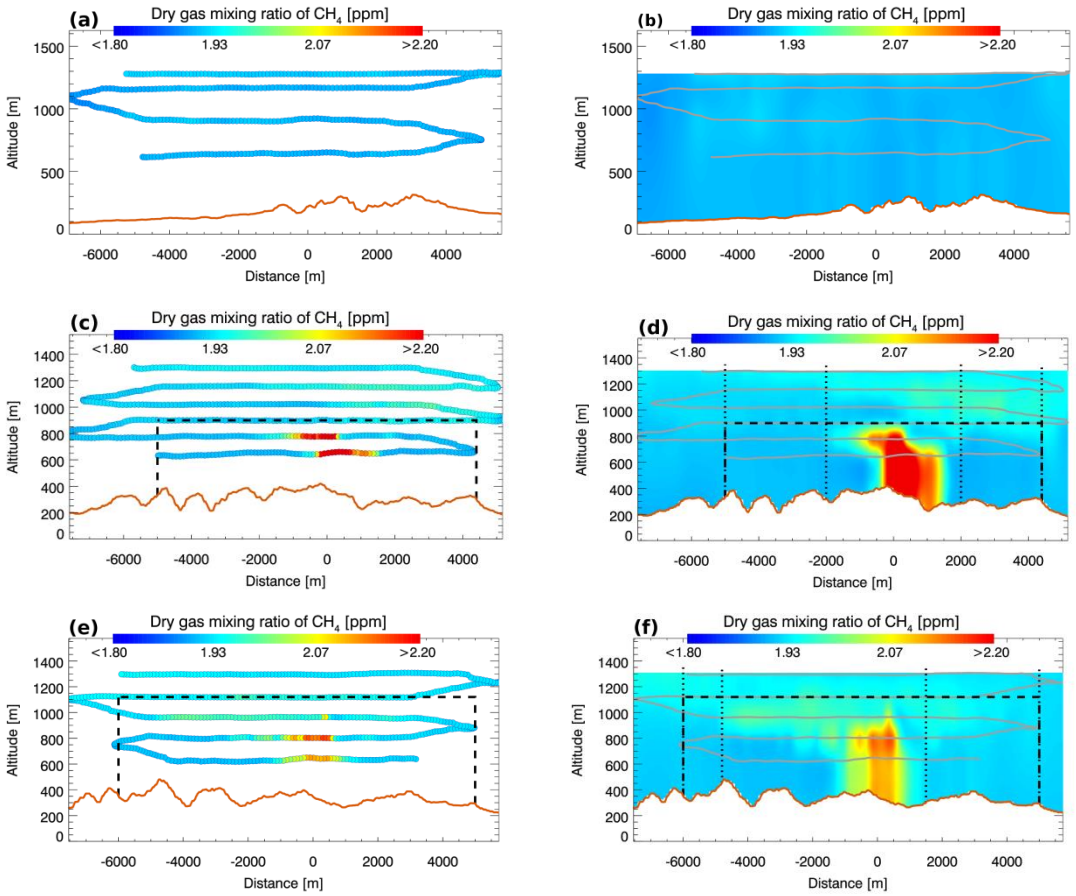

Figure S 7. As for Fig. S5 but for the 01.09.2014. (a,b) Upwind wall. (c,d) First downwind wall. (e,f) Second downwind wall.

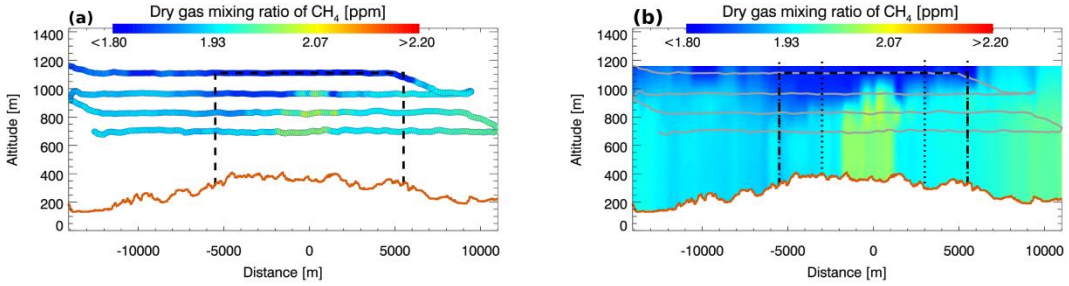

Figure S 8. As for Fig. S5 but for the 03.01.2014. (a,b) Downwind wall.

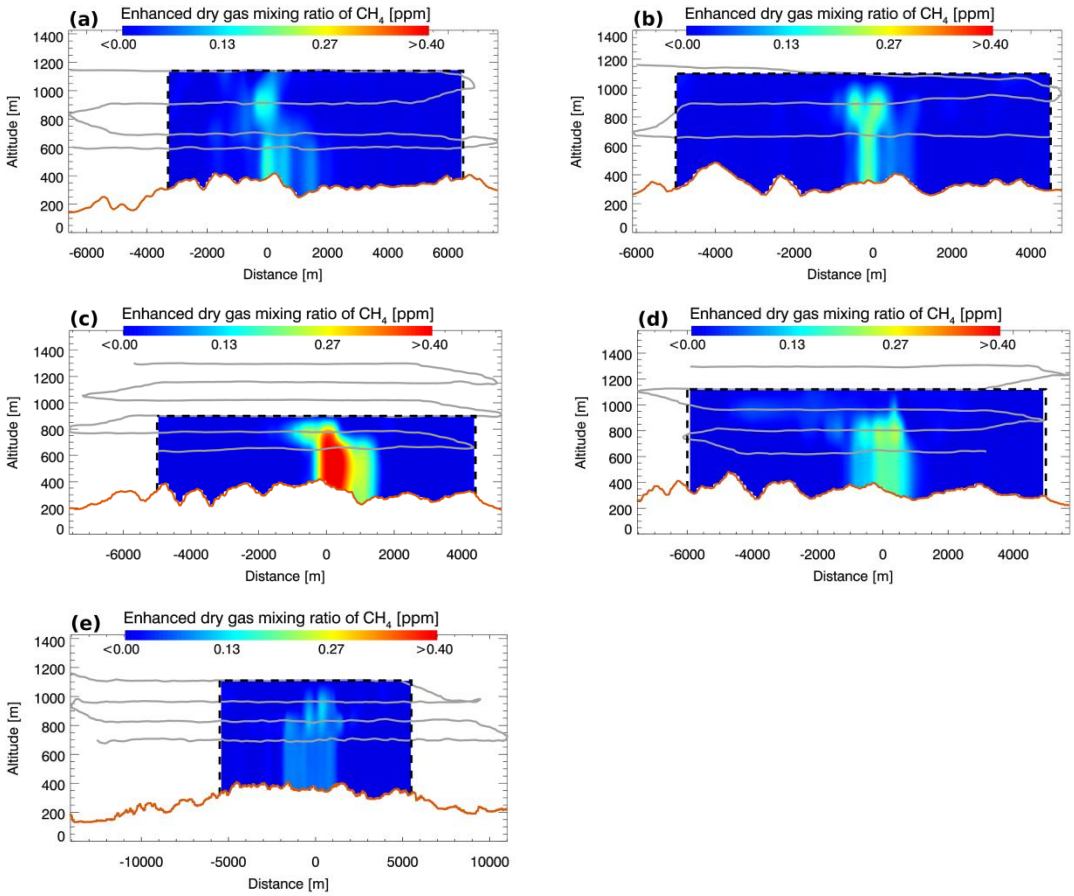

Figure S 9. Shown are enhanced dry gas mixing ratios of CH_4 of the five downwind walls acquired on the four different flight days 27.08.2014 (a), 28.08.2014 (b), 01.09.2014 (c, first downwind wall; d, second downwind wall) and 03.09.2014 (e). Only the area, which was used in the mass balance approach, is shown (dashed black line). Solid orange line depicts the surface elevation at the position of the wall (based on SRTM). Solid grey line shows the flight track.

S3 Picarro in-situ dry gas mixing ratios of CO_2

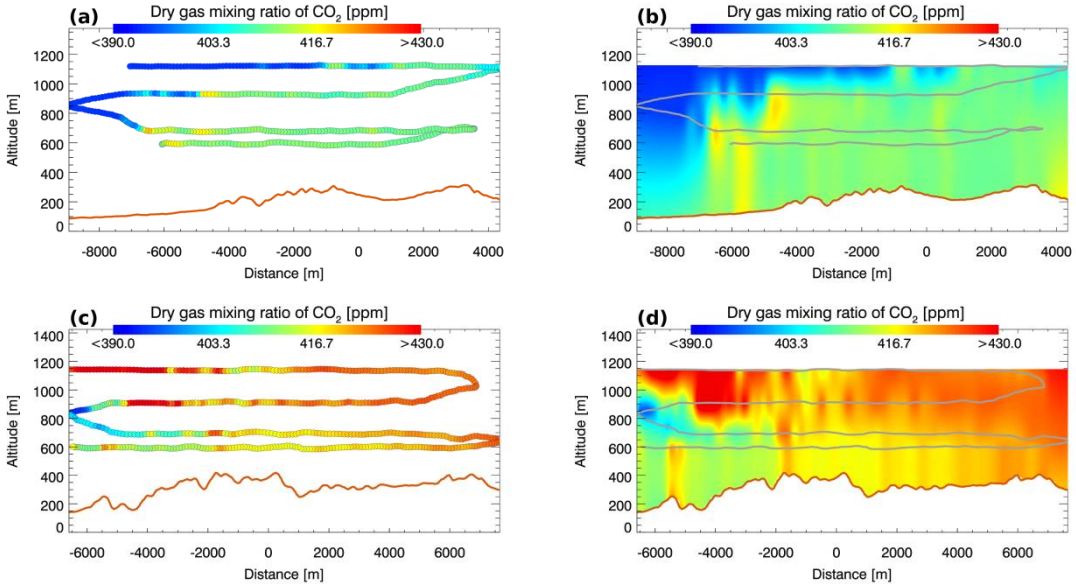

Figure S 10. As Fig. S5 but for the dry gas mixing ratios of CO_2 on 27.08.2014 and without dashed and dotted lines. (a,b) Upwind wall. (c,d) Downwind wall.

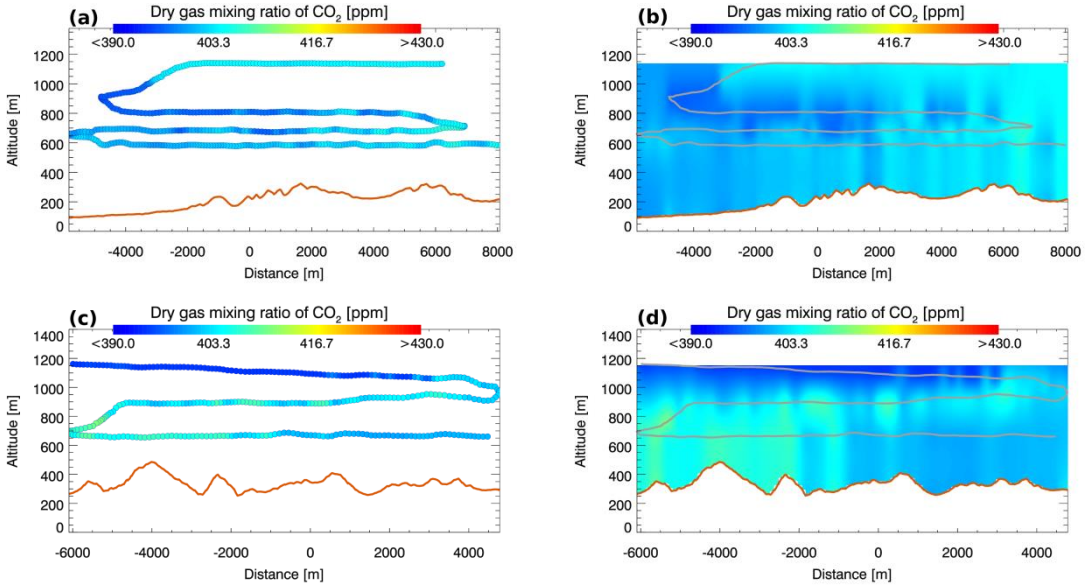

Figure S 11. As for Fig. S10 but for the 28.08.2014. (a,b) Upwind wall. (c,d) Downwind wall.

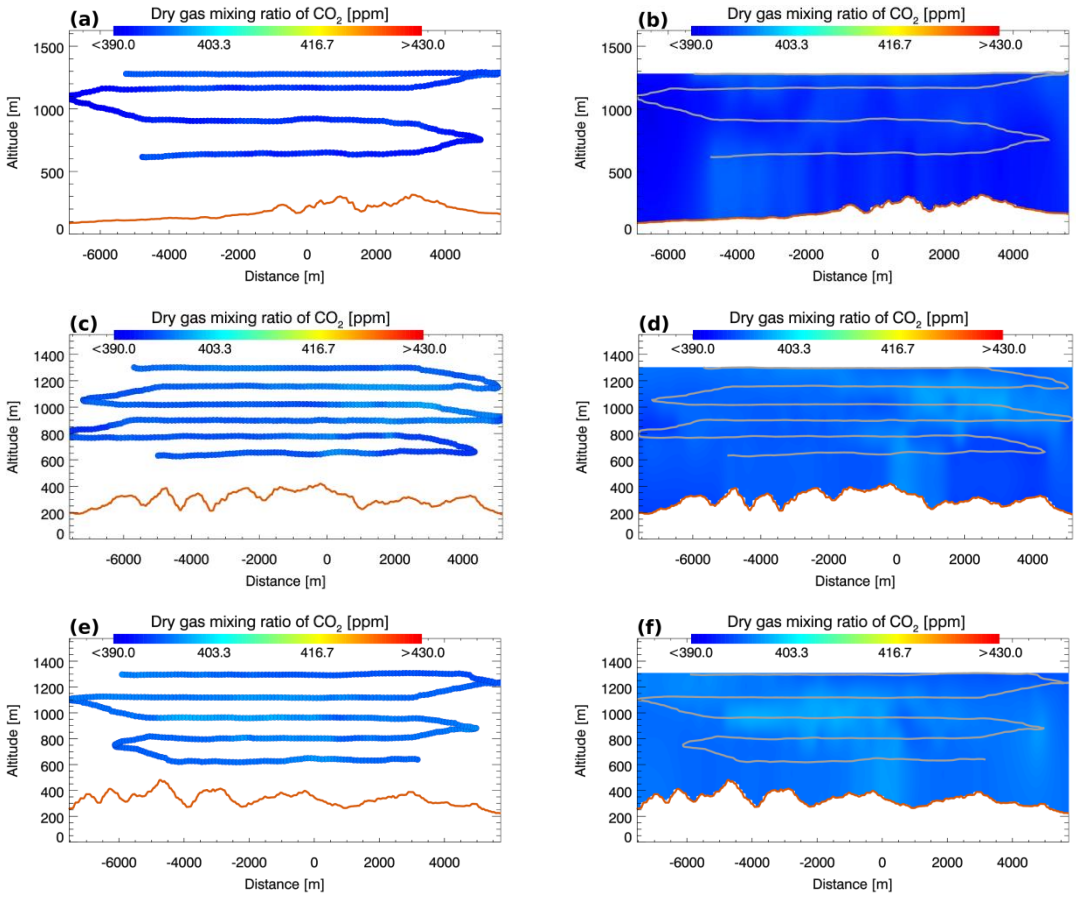

Figure S 12. As for Fig. S10 but for the 01.09.2014. (a,b) Upwind wall. (c,d) First downwind wall. (e,f) Second downwind wall.

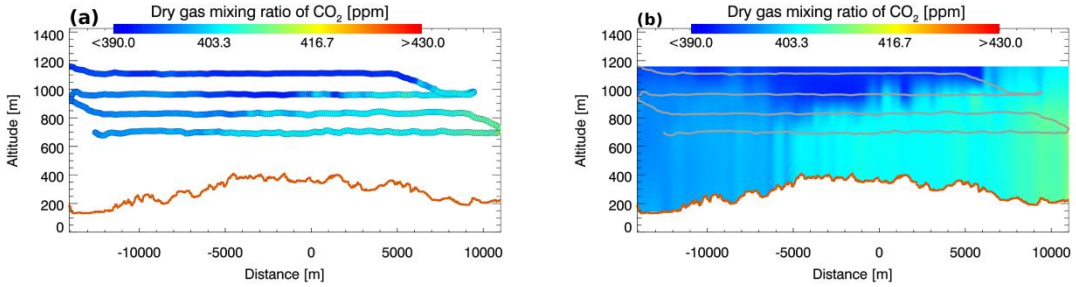

Figure S 13. As for Fig. S10 but for the 03.01.2014. (a,b) Downwind wall.

S4 Horizontal wind fields u_{eff} used in the mass balance approach

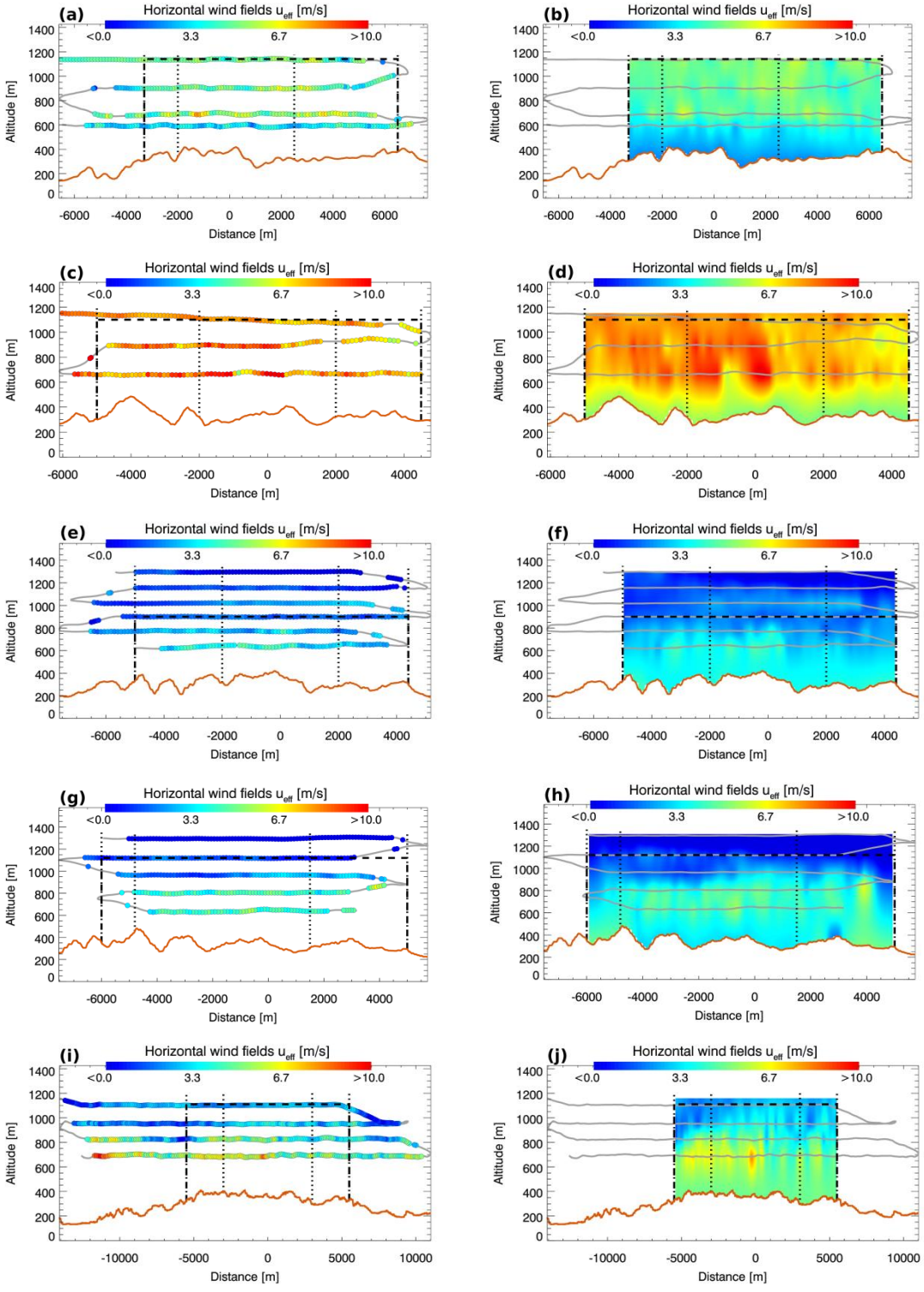

Figure S 14. Shown are the horizontal wind fields u_{eff} of the five downwind walls used in the mass balance approach acquired on the four flight days 27.08.2014 (a,b), 28.08.2014 (c,d), 01.09.2014 (e,f, first downwind wall; g,h, second downwind wall) and 03.09.2014 (i,j). Measurements are filtered by an inclination of 5° (see also main text). The area used in the mass balance approach is bordered by a dashed black line. Dotted black line shows limits, which were used to define the CH_4 background area. Solid orange line depicts the surface elevation at the position of the wall (based on SRTM). Solid grey line shows the flight track.

S5 Integrated in-situ columns (IISC)

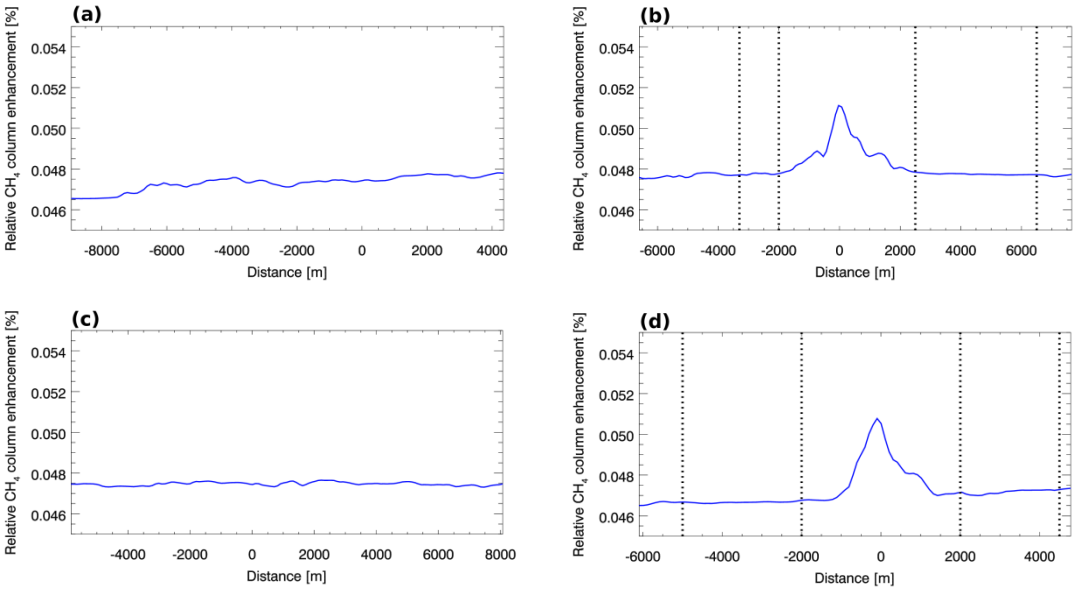

Figure S 15. Ratios of the integrated in-situ columns of CH_4 and CO_2 for the upwind walls (a,c) and downwind walls (b,d) on the 27.08.2014 (a,b) and 28.08.2014 (c,d). The measurements enclosed by the black dotted lines and located at the flanks / edges of the plume are used for normalisation (compare to Fig. S17).

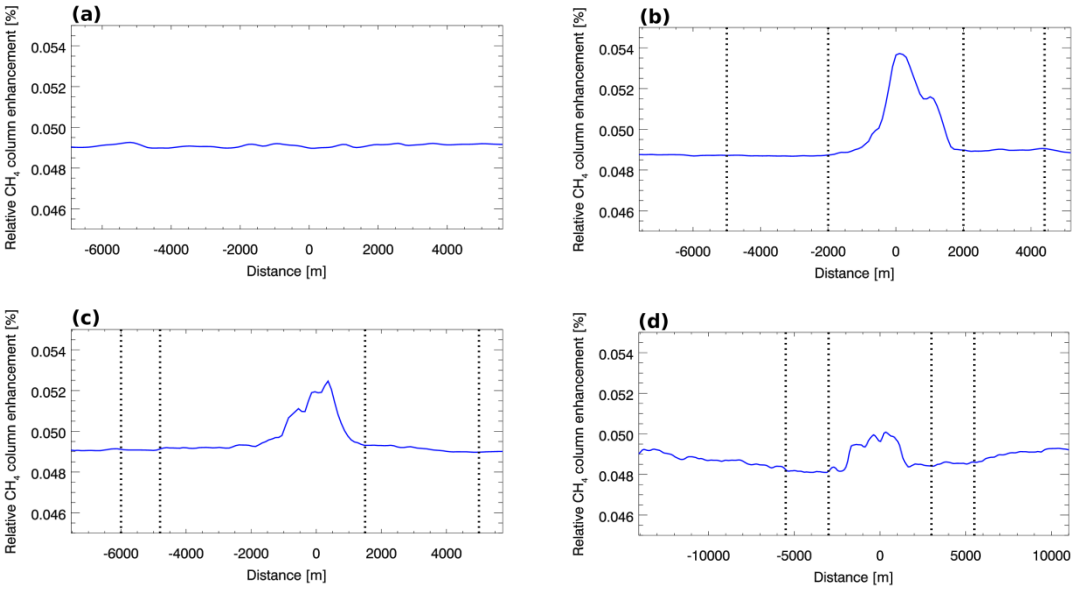

Figure S 16. As Fig. S15 but for the upwind wall (a), first downwind wall (b) and second downwind wall (c) on the 01.09.2014 and the downwind wall (d) on the 03.09.2014 (also compare to Fig. S17).

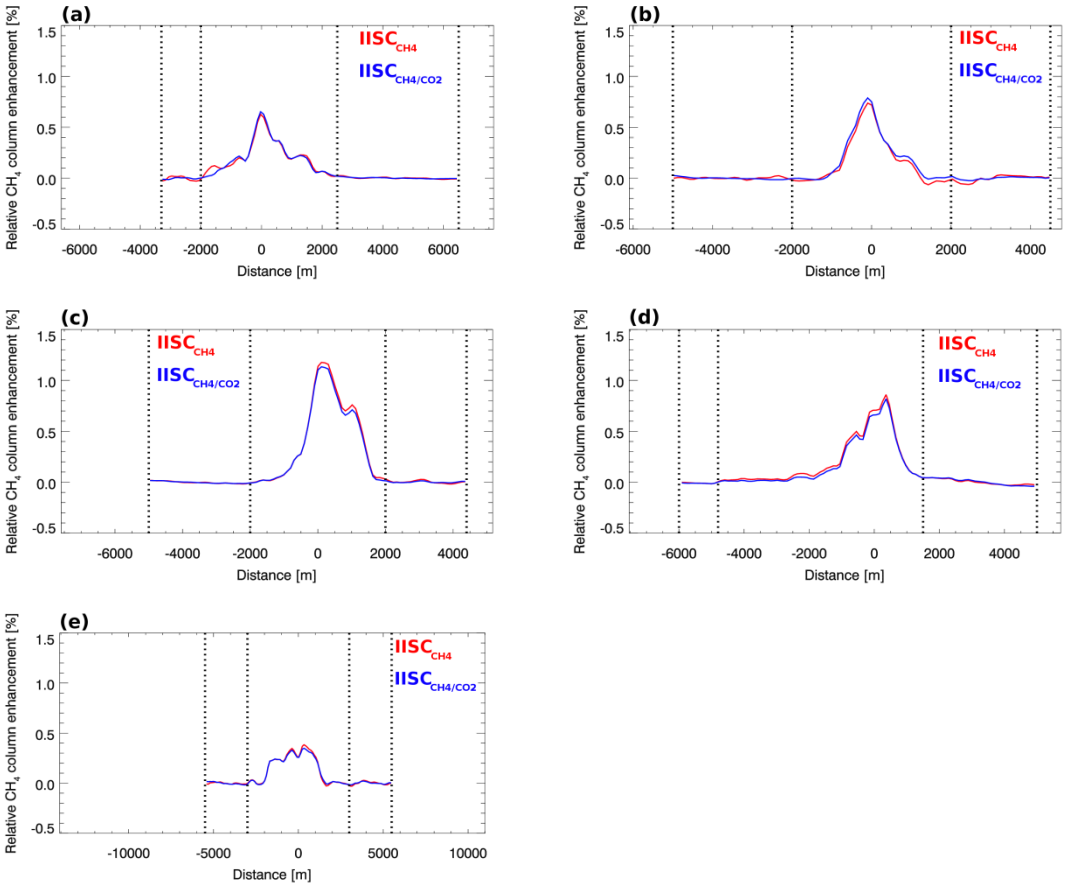

Figure S 17. As Fig . 8 in the main part but for all downwind walls. (a) 27.08.2014. (b) 28.08.2014. (c) 01.09.2014, first downwind wall (as in Fig. 8, a). (d) 01.09.2014, second downwind wall (as in Fig. 8, b). (e) 03.09.2014.

S6 AVIRIS-NG CH_4 retrieval results (Google Earth overlays)

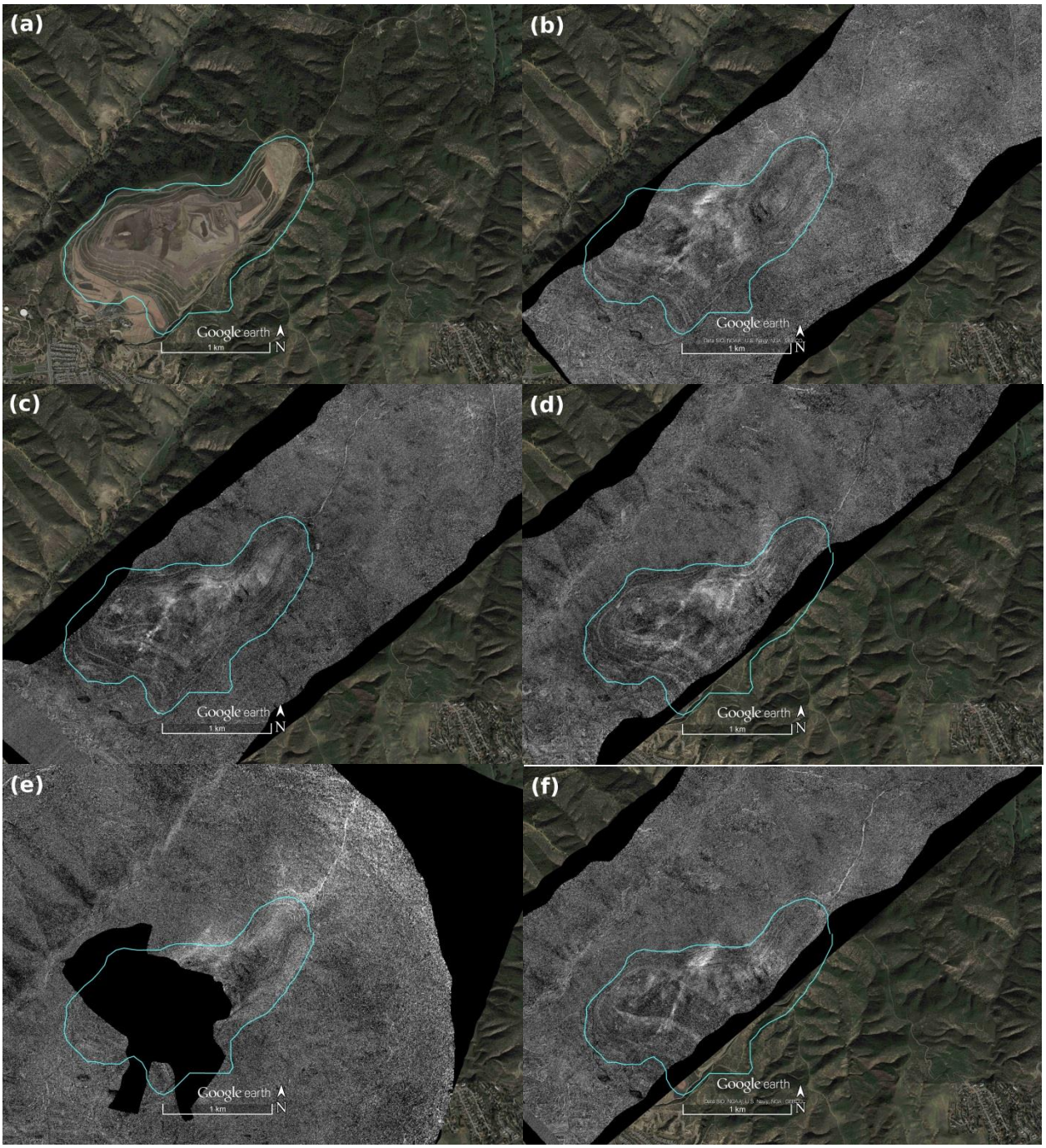

Figure S 18. Overview of the methane retrieval results from the AVIRIS-NG observations from different overflight times [local time]: a) Underlying Google Earth Map of the Olinda Alpha Landfill which is emphasized by the cyan solid line. (b) 13:31. (c) 13:33, same overflight as shown in Fig. 9 in the main part. (d) 13:38. (e) 13:48. (f) 14:06.

S7 Vertical background profiles of CO_2 and CH_4

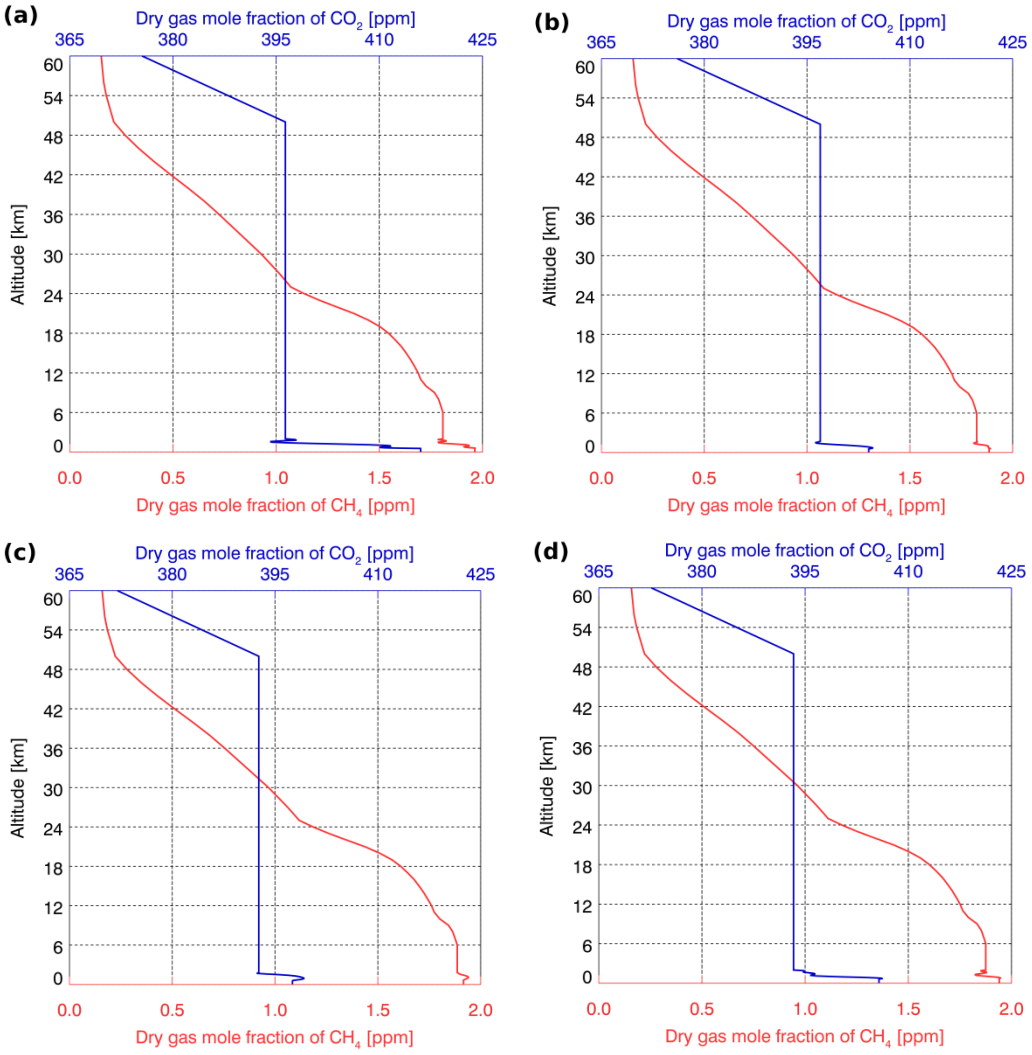

Figure S 19. Shown are the scaled background profiles (as described in Sect. 3.1 of the main manuscript), which were used in the MAMAP remote sensing retrieval: (a) 27.08.2014. (b) 28.08.2014. (c) 01.09.2014. (d) 03.09.2014

S8 Observation System Simulation Experiment (OSSE)

Observation System Simulation Experiments (OSSEs) can be used to simulate the propagation of plumes in the atmosphere originating from various source types and how these plumes would look like if they were measured by, e.g., the MAMAP remote sensing instrument. That means they can be used to qualitatively estimate whether an emission source is observable with the MAMAP remote sensing instrument considering prevailing atmospheric conditions as well as instrumental and flight specific characteristics. The method discussed in the following has been used to estimate, for example, upper-limit emission rates of CH_4 for a blowout site located in the North Sea (Gerilowski et. al., 2015) and is based on vertically integrated Gaussian plume forward model simulations (for details, see Krings et. al., 2011 and Gerilowski et al., 2015):

$$V(x,y) = \sum_{i=1}^{N} \frac{F_i}{\sqrt{2\pi}\,\sigma_y(a,x_i)u}\ \exp\left(-\frac{1}{2}\left(\frac{y_i}{\sigma_y(a,x_i)}\right)\right) \qquad \text{Eq. S1}$$

where $V(x,y)$ is the vertically integrated column, which is subsequently normalized by the background column to achieve, e.g., the desired CH_4 variation relative to the background column, as a result of one or more emission sources i having emission rates F_i, u is the prevailing wind speed which is assumed to be constant across the entire simulation and measurement area, respectively, $\sigma_y(a,x_i)$ is the horizontal dispersion coefficient in across wind direction with the parameter a depending, in a first order approximation, on wind speed and solar insolation, x_i is the along wind coordinate and y_i the across wind coordinate of source i. The sigma sign indicates the summation over all possible sources i.

In order to simulate emissions from the landfills under investigation, it was assumed that CH_4 emissions took place homogenously distributed across the entire landfill. Therefore, depending on the shape and size of the landfill 90 to 100 single sources were homogenously distributed across the landfill area. Table S1 summarises the parameters necessary for the simulations of the four landfills shown in Fig. 1 in the main manuscript. As these simulations are compared to the actual MAMAP remote sensing measurements, all parameters were derived from the corresponding measurement flights. In order to estimate the wind directions and wind speeds at the BKK Landfill (BKK), Puente Hills Landfill (PHL) and Scholl Canyon Landfill (SCL) sites, we assumed the same vertical wind profile as measured for the Olinda Alpha Landfill (OAL) flight on the corresponding day, but scaled based on a comparison of the surface winds measured by weather stations at the time, the landfills were surveyed. The BKK and PHL are close to the OAL. Therefore, the weather station at the OAL was used to estimate their surface winds. For the SCL, we used the weather station KCAGLEND17 (https://www.wunderground.com/personal-weather-station/dashboard?ID=KCAGLEND17#history/tgraphs/s20140827/e20140827/mdaily) close to this landfill site. For the simulation of, e.g., the BKK Landfill on the 01.09.2014, the surface wind speed and, thus, the wind speed used for the simulation, was the same as for the subsequent OAL flight (4.4 ms^{-1}). The EPA emission rate estimate is 15.1 $ktCH_4yr^{-1}$ for 2014, which was equally distributed over the approximate 100 sources. The parameter a used for the horizontal dispersion coefficient σ_y is based on the atmospheric stability classification (Turner, 1970) using the wind speed and solar insolation. Thus, a wind speed of 4.4 ms^{-1} and strong solar insolation results in stability class B corresponding to a value of a = 156 (Martin, 1976).

	BKK, 01.09.2014	SCL, 27.08.2014	PHL, 27.08.2014	OAL, 01.09.2014
Time of overflight	14:26 – 14:54	11:27 – 12:03	12:17 – 13:20	14:55 – 16:05
Emission rate [$ktCH_4yr^{-1}$]	15.1	5.9	5.0	14.3
Surface area [km^2]	1.4	0.85	2.4	1.7
Stability class	B	A - B	B	B
Parameter a	156	185	156	156
Wind speed [ms^{-1}]	4.4	2.5	4.0	4.4
Wind direction [°]	235	210	227	238
Ground scene size [m^2]	69 x 69	63 x 63	46 x 46	64 x 64
Precision [%]	0.30	0.27	0.33	0.34

Table S1: Summery of the relevant quantities used in the Observation System Simulation Experiments (OSSEs).

Figure S20 (a) shows such a simulation for the BKK Landfill. The resulting column enhancement has also been gridded to pixels having the same size as the approximate ground scene size of the MAMAP remote sensing flight on that day (~ 69 x 69 m^2) for better comparison. The simulated plume has additionally been rotated in the prevailing wind direction (235°). In the next step (Fig. S20, b), a noise component was added to the simulation to replicate the single measurement precision of the MAMAP remote sensing instrument. The noise was calculated as 1-σ standard deviation (0.30%) from the actual MAMAP remote sensing measurements over the BKK Landfill. In the final step (Fig. S20, d), simulated grid points were only plotted if the MAMAP instrument also gathered data at the specific positions, that is: along the flight track. For comparison, the actual MAMAP flight track over the BKK Landfill on the 01.09.2014 is shown in Fig. S20 (c). From that, one concludes that if the BKK landfill had emitted 15.11 $ktCH_4yr^{-1}$ at the time of the measurement, it should likely have been observable by the MAMAP remote sensing instrument (for details, see also main text). The comparison of measurements and simulations for the Scholl Canyon Landfill and Puente Hills Landfill are shown in Fig. S21, and for the Olinda Alpha Landfill in Fig. 12 in the main manuscript (Sect. 4.7, including also the conclusions from these experiments).

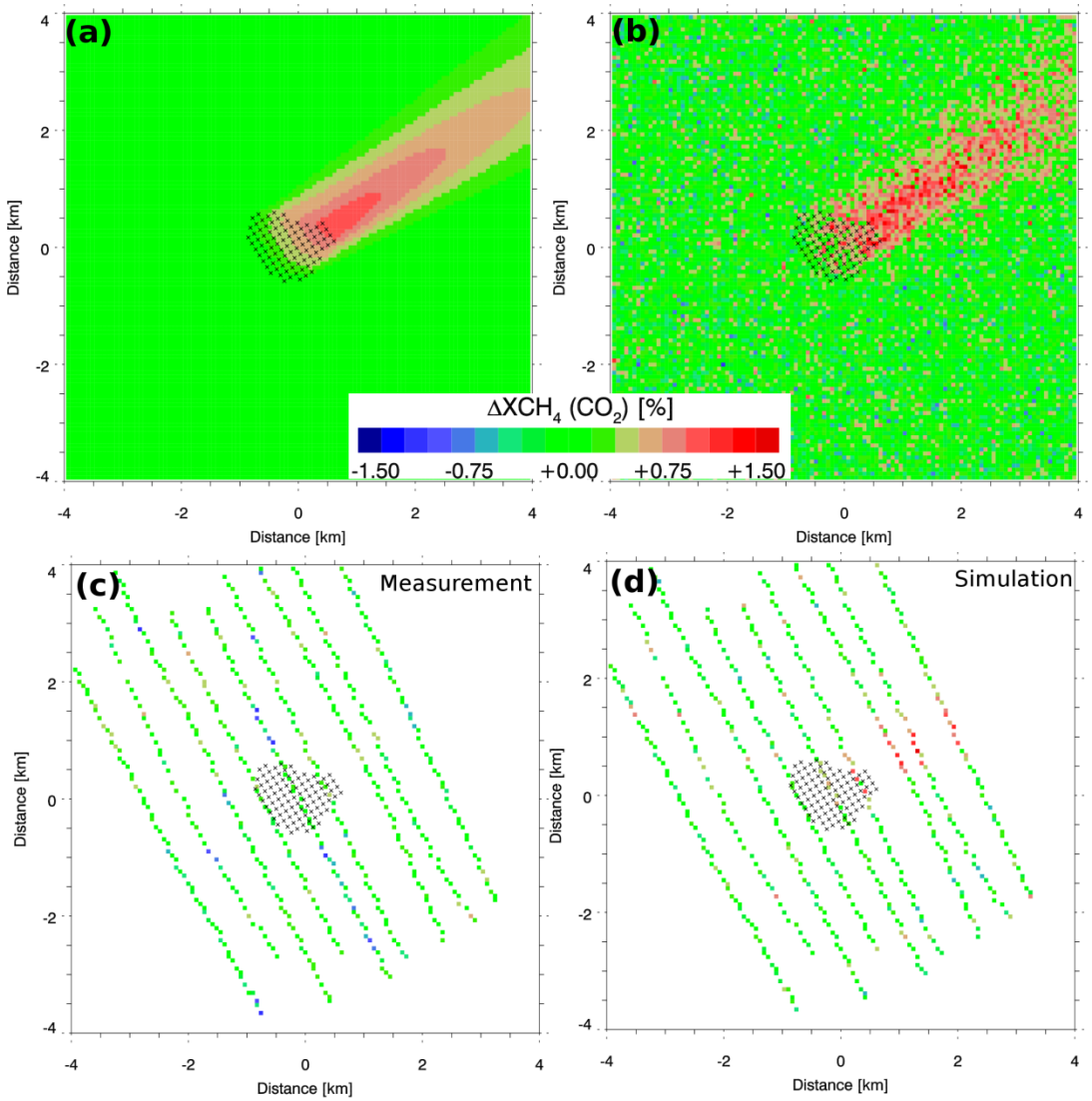

Figure S 20. (a) Shows the CH_4 variation relative to the background column for the BKK Landfill on the 01.09.2014 based on the OSSE. (b) Shows the same as (a) but with an added noise component. (d) Shows the OSSE only at the position where actual measurement have been acquired. (c) Actual measurement of the MAMAP remote sensing instrument.

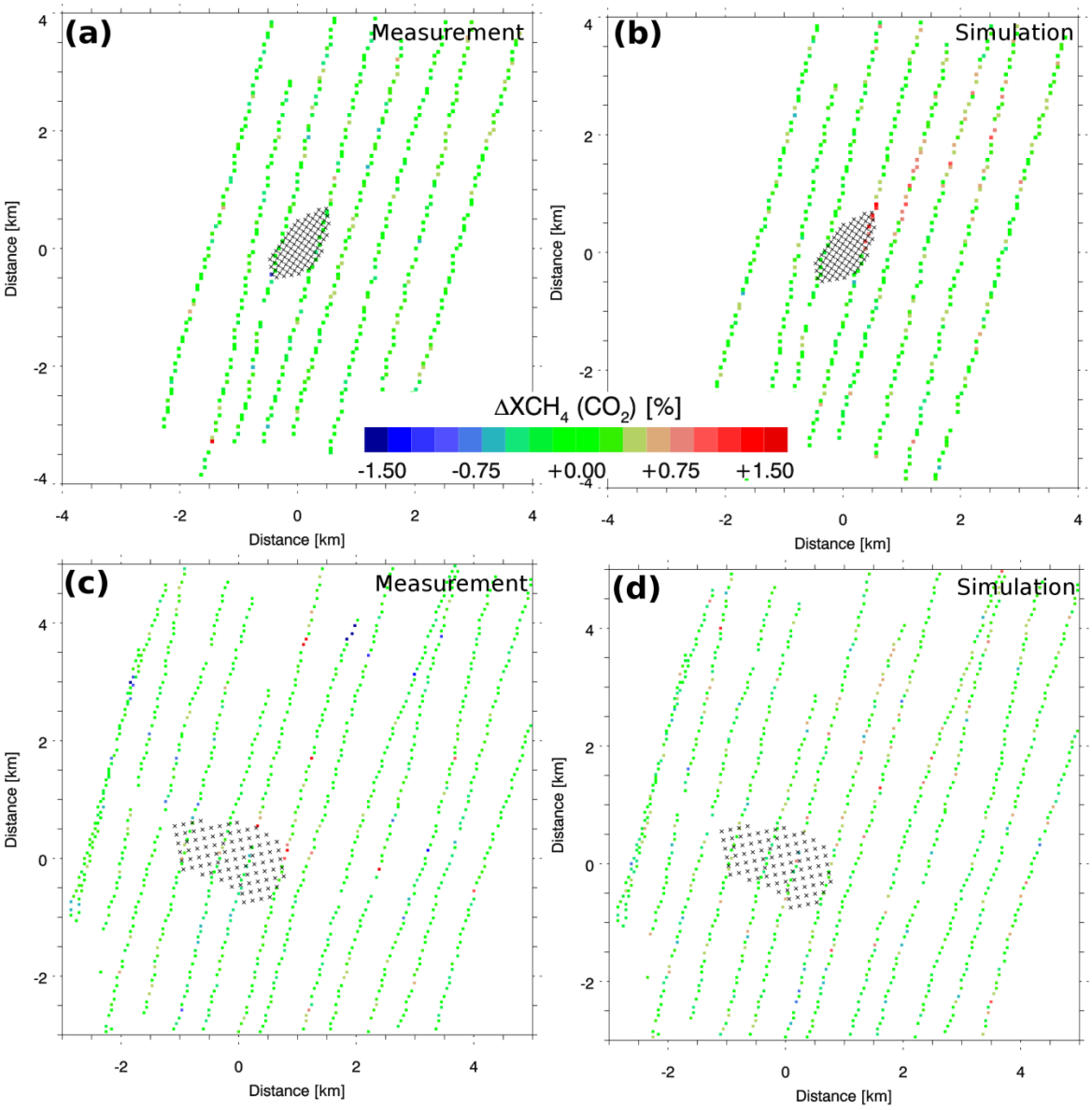

Figure S 21. As Fig. 12 but for the SCL on the 27.08.2014 (a,b) and for the PHL on the 27.08.2014 (c,d).

S9 Landfill reporting practice in the U.S.

In the U.S., landfill operators need to report landfill emissions, in case the landfill is equipped with a gas collection system, in two different ways to the United States Environmental Protection Agency (GPO, 2013). The first approach (A1, forward calculation approach) is driven by model data using, e.g., the type and amount of waste, which has historically been deposit within a landfill in combination with a first order decay model. The second approach (A2, back calculation approach) is driven by measurements of the amount of CH_4, which has been recovered by the gas collection system, and gas collection efficiencies to estimate CH_4 emissions. The official value stated by EPA always represents the larger estimate of the two.

The landfills Olinda Alpha (OAL), BKK, Scholl Canyon (SCL) and Puente Hills (PHL) investigated in this work are equipped with a gas collection system. An overview of the reported emission rates of the four landfills between 2010 and 2015 is given in Table S2.

		2010	2011	2012	2013	2014	2015
OAL							
Emission in $ktCH_4yr^{-1}$	Official	13.2	15.4	14.7	14.3	11.5	12.3
	A1	11.2	5.9	9.3	10.4	10.0	12.3
	A2	13.1	15.4	14.7	14.4	11.5	9.2
BKK							
Emission in $ktCH_4yr^{-1}$	Official	14.1	13.6	14.6	15.0	15.1	15.1
	A1	14.1	13.6	14.6	15.0	15.1	15.1
	A2	1.3	1.3	1.2	1.0	0.9	0.9
SCL							
Emission in $ktCH_4yr^{-1}$	Official	5.6	6.9	6.5	6.3	5.9	5.3
	A1	0.0	0.0	0.0	1.0	2.1	3.2
	A2	5.6	6.9	6.5	6.3	5.9	5.3
PHL							
Emission in $ktCH_4yr^{-1}$	Official	17.8	17.2	17.2	10.9	5.0	13.4
	A1	8.3	4.1	4.2	7.7	2.4	13.3
	A2	17.8	17.2	17.2	10.9	5.0	4.4

Table S2: Reported emission rates of the four landfills: Olinda Alpha Landfill (OAL), BKK Landfill (BKK), Scholl Canyon Landfill (SCL), Puente Hills Landfill (PHL). The emission rates for the year 2014 are emphasized in yellow. For each landfill and year three emission rates are given: Official (officially reported by EPA), A1 (forward calculation approach) and A2 (back calculation approach, GPO, 2013).

The emission data for the different facilities and landfills, respectively, from Table S2 can be found at the EPA website: https://ghgdata.epa.gov/ghgp/main.do, last access: 09.06.2017.
OAL: https://ghgdata.epa.gov/ghgp/service/facilityDetail/2014?id=1002320&ds=E&et=&popup=true, last access: 09.06.2017.
BKK: https://ghgdata.epa.gov/ghgp/service/facilityDetail/2014?id=1011449&ds=E&et=&popup=true, last access: 09.06.2017.
SCL: https://ghgdata.epa.gov/ghgp/service/facilityDetail/2014?id=1003198&ds=E&et=&popup=true, last access: 09.06.2017.
PHL: https://ghgdata.epa.gov/ghgp/service/facilityDetail/2014?id=1003199&ds=E&et=&popup=true, last access: 09.06.2017.

References

Gerilowski, K., Krings, T., Hartmann, J., Buchwitz, M., Sachs, T., Erzinger, J., Burrows, J. P., and Bovensmann, H.: Atmospheric remote sensing constraints on direct sea-air methane flux from the 22/4b North Sea massive blowout bubble plume, Marine and Petroleum Geology, 68, 824–835, doi:10.1016/j.marpetgeo.2015.07.011, 2015.

GPO: U.S. Government Publishing Office; U.S. Environmental Protection Agency: Rules and Regulations; Federal Register; Vol. 78; No. 230, available at http://www.gpo.gov/fdsys/pkg/FR-2013-11-29/pdf/2013-27996.pdf, last access: 15.05.2017, 2013.

Krings, T., Gerilowski, K., Buchwitz, M., Reuter, M., Tretner, A., Erzinger, J., Heinze, D., Pflüger, U., Burrows, J. P., and Bovensmann, H.: MAMAP - a new spectrometer system for column-averaged methane and carbon dioxide observations from aircraft: retrieval algorithm and first inversions for point source emission rates, Atmospheric Measurement Techniques, 4, 1735–1758, doi:10.5194/amt-4-1735-2011, 2011.

Martin, D. O.: Comment On"The Change of Concentration Standard Deviations with Distance", Journal of the Air Pollution Control Association, 26, 145–147, doi:10.1080/00022470.1976.10470238, http://dx.doi.org/10.1080/00022470.1976.10470238, 1976.

Turner, D. and Administration, U. S. N. A. P. C.: Workbook of Atmospheric Dispersion Estimates, Environmental health series: Air pollution, U.S. Department of Health Education and Welfare, Public Health Service, Environmental Health Service, National Air Pollution Control Administration, 1970.